Robust Reset Speed Synchronization Control for an Integrated Motor-Transmission Powertrain System of a Connected Vehicle Under a Replay Attack

Xiangyang Xu, Xiang Li, Peng Dong, Yue Liu, and Hui Zhang, *Senior Member, IEEE*

***Abstract*—This paper deals with the speed synchronization control of a connected vehicle subject to a replay attack. A large number of replay attack signals are injected into controller area network (CAN) through external network, which greatly reduces the real-time control performance of a connected integrated motor-transmission (IMT) system. In order to ensure the performance of an IMT speed tracking system under large random message delays, a robust reset controller combined with a delay-robust speed synchronization controller satisfying energy-to-peak performance is designed in this paper. The uncertain impact caused by a replay attack is described by large random network delays which are modeled by polytopic inclusion. Then, a dynamic output-feedback controller considering the uncertainty caused by attack-delays is proposed for online speed tracking. Moreover, a robust reset controller is designed to obtain comparatively better transient response in the case of large attack-delays. In this control strategy, once the reset condition is triggered, the after-reset value calculated by linear matrix inequalities (LMIs) would replace the dynamic state vector. Finally, the effectiveness of the proposed controller is verified by comparing it with model predictive control (MPC), existing PD control considering delays and energy-to-peak robust control in terms of performance.**

***Index Terms*—Integrated motor-transmission (IMT) powertrain, energy-to-peak robust control, reset control, attack-induced delays, replay attack.**

I. Introduction

With the development of connected vehicles and the advancement of communication technologies, the connection through external communication networks and in-vehicle controller area network (CAN) provides drivers enjoyable driving environment and economical driving guidance [1]–[3]. Once the vehicle is connected to the external network, there are two kinds of communication networks. One is the external network which transmits instructions from remote servers to vehicles and the other one is the CAN which helps the communication between control signals and sensor measurement signals [4].

Unfortunately, malicious components and malicious programs embedded in CAN as well as wireless interfaces all provide opportunities for attackers to invade an in-vehicle CAN. Moreover, CAN data frames without authentication will be broadcast to each network node, paving the way for an attacker to eavesdrop or launch an attack on the vehicle control system. Extensive experiments proved that attackers use the in-vehicle CAN as an entry point to attack vehicles [5]–[8]. Besides, Murvay and Groza have carried out a replay attack, a denial of service (DoS) and a distributed DoS attack experiment on a commercial vehicle with SAE J1939 [9]. Kang et.al have developed an automated CAN analyzer (ACA) which supported the execution of a deception attack [10]. Road tests conducted by Koscher *et al.* show that by using the on-board diagnostics (OBD) tool to insert malicious components or inject malicious programs on CAN, an attacker can shut down the brakes and stop the engine [11]. Woo *et al.* and Choi *et al.* have carried out a long-range wireless replay attack experiment by using a real vehicle and malicious smartphone applications [12]. Based on the above attack experiments, published results analysed the CAN security vulnerability and proposed some effective protocols to filter attack signals [12]–[15]. In practice, attack signals increase CAN bus load and take up the transmission time of legitimate signals. Security protocols protect information security, while the response of control system under attack-delays needs to be improved.

The unknown time-varying delays on in-vehicle CAN may downgrade the real-time performance of CAN message transmission, which presents a challenge to controller design [16]–[18]. Numerous studies have discussed the system stability with short time-varying delays. Banos, Liu *et al.* studied the theoretical stability conditions of the reset control system under time-varying delays [19]–[24]. In vehicle system control, integrated motor transmission (IMT) powertrain system with directly combined a motor and a gearbox has shown the great potential to be one of the best transmission mechanisms for connected vehicles [25]–[32]. Moreover, the IMT speed tracking controller considering short time-varying delays has been studied deeply. Caruntu *et al.* pointed out that the CAN message delay is one of the factors causing the oscillation of the IMT

Manuscript received January 3, 2020; revised April 30, 2020 and July 6, 2020; accepted August 16, 2020. Date of publication September 1, 2020; date of current version July 8, 2021. This work was supported in part by the National Natural Science Foundation of China under Grants U1664257 and U1864201, in part by the Vehicle Power Specific Research Project of Fundamental Product Innovation Program under Grant JCCPCX201704, in part by National Key R&D Program of China under Grant 2018YFB0105900, and in part by the 2025 Science and Technology Innovation Program of Ningbo under Grant 2019B10111. The review of this article was coordinated by Prof. Sukumar Kamalasadan. *(Corresponding author: Hui Zhang.)*

The authors are with the School of Transportation Science, and Engineering, Beihang University, Beijing 100191, China, and also with the Ningbo Institute of Technology, Beihang University, Ningbo 315323, China (e-mail: xxy@buaa.edu.cn; Xiang_Li@buaa.edu.cn; dongpengbeihang@163.com; sy1613207@buaa.edu.cn; huizhang285@gmail.com).

Digital Object Identifier 10.1109/TVT.2020.3020845

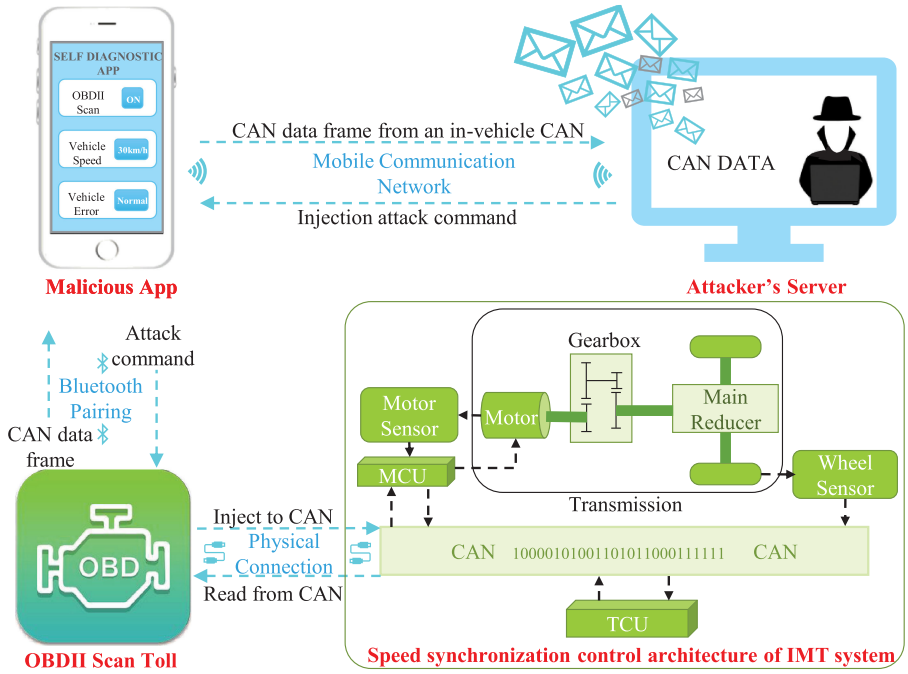

Fig. 1. Replay attack process to a connected IMT speed synchronization control system.

transmission system [33]. Zhu *et al.* proposed a robust IMT speed tracking controller and reduced powertrain oscillation caused by network-induced time-varying delays [34]. Based on his study, Li *et al.* proposed a dynamic output-feedback controller to resist time-varying delay [35]. Xu *et al.* proposed an event-triggered controller to reduce the network congestion of an IMT speed tracking system [36]. Liu *et al.* proposed an approach for robust mixed H_∞/LQR controller for an IMT speed tracking system [37]. An active CAN period-scheduling approach was designed to govern the utilization of in-vehicle CAN and thus enhance IMT speed tracking performance [38]. These controllers achieved good speed tracking performance when the CAN-induced delays were less than twice of the sampling time.

The large random attack-induced delays may cause some controllers to be infeasible. Fortunately, the controllers proposed in [34] and [37] can reduce the impact. However, such controllers lead to comparatively worse performance regarding speed tracking response and oscillation damping capability. Therefore, some countermeasures need to be applied to address it. The reset controller is a type of hybrid controller that the state variables of the controller are reset when certain predefined constraints are met. Thus more degrees of freedom of the controller appear and they could be used to achieve the trade-off between fast response time and small overshoot [39], [40]. Based on the above consideration, a controller combing reset control and delay robust control techniques, referring to [34], is designed in this paper to ensure the speed tracking performance and oscillation damping capability under delays induced by a replay attack. A new method of obtaining after-reset values is proposed instead of a traditional zero-crossing. The after-reset value is obtained by minimizing a quadratic cost function based on a model predictive control (MPC) method [41], [42].

In this paper, a dynamic output-feedback robust controller satisfying energy-to-peak performance combined with a robust reset controller is designed to preserve the oscillation damping capability and improve the speed tracking capability of a connected car under a replay attack. The main contributions of our research are listed in the following respects. 1) A adjustable dynamic tracking controller is proposed, rendering the closed-loop control system robust to uncertain time-varying delays. 2) A robust reset controller is designed to calculate the after-reset value online by considering the stability of the reset control system with time-varying delays. 3) The real-time online calculation, speed tracking and oscillation damping capability of the proposed controller are verified by a hardware-in-the-loop (HIL) online experiment. The experiment results show that the overshoot and settling time of the proposed controller is 25.9% and 25.1% less than these performance indexes in [34] under step response test conditions from 7 km/h to 20 km/h under a replay attack with random time-varying delays up to 100 ms.

II. Problem Formulation

A. Replay Attack Model

Fig. 1 shows a replay attack process at an IMT transmission system, which can be divided into a speed synchronization control process of the IMT system and a process of eavesdropping and attacking in-vehicle CAN data.

As illustrated in Fig. 1, the speed synchronization control architecture of an IMT system consists of a motor, a gearbox, a drive shaft, wheels, a transmission control unit (TCU), an motor control unit (MCU) and a CAN communication network. A TCU is employed for speed synchronization control and an MCU is applied to help the motor accurately execute torque commands from the TCU. In this paper, we consider an attack process on

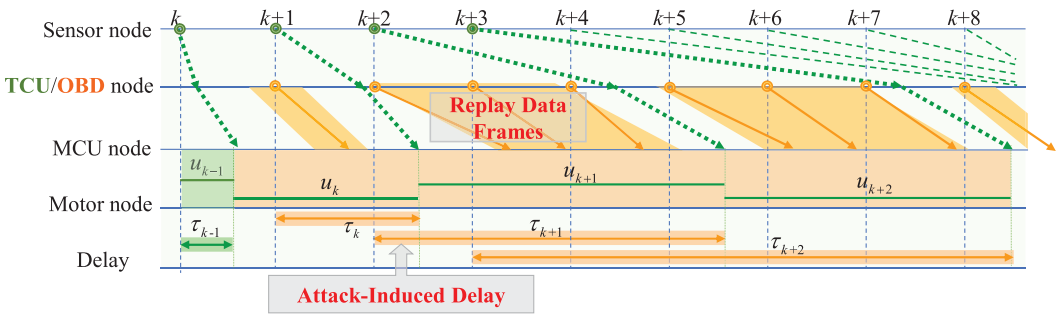

Fig. 2. The schematic diagram of CAN data transmission under a replay attack.

CAN, similar as the replay attack addressed in [43]. In such a process setup, an OBDII scan toll connects with the in-vehicle CAN through a physical interface. All data frames are broadcasted to every in-vehicle CAN node. Therefore, the OBDII node could eavesdrop CAN data frames and send these data to the self-diagnostic APP and the attacker. Moreover, the OBDII scan toll could retransmit these eavesdropped data into the in-vehicle CAN masquerading as a diagnostic process at attacker's request. In fact, malicious self-diagnostic APPs that control the OBDII tools through bluetooth and communicate with attackers over mobile network are allowed to be downloaded from APP market. If the victim downloads them, eavesdropping and attacking the in-vehicle CAN will be implemented.

B. Description of Attack-Induced Time-Varying Delays

Fig. 2 demonstrates the impact of replay attack signals on legitimate CAN messages transmission. The TCU control signals retransmitted by the malicious OBDII node will not be executed with the security protocol in [12]. However, Fig. 2 shows that these random attack signals greatly increase CAN messages transmission time.

C. Fundamentals of an IMT System

The state-space model of an IMT system is expressed as [34].

$$\dot{x} = A_c x + B_{u,c} u + B_{\omega,c}\omega \tag{1}$$

where $A_c = \begin{bmatrix} -\frac{c_m}{J_{mg}} - \frac{c_f}{i_g^2 i_0^2 J_{mg}} & \frac{c_f}{i_g i_0 J_v} & -\frac{k_f}{i_g i_0 J_v} \\ \frac{c_f}{i_g i_0 J_v} & -\frac{c_a + c_f}{J_v} & \frac{k_f}{J_v} \\ \frac{1}{i_g i_0} & -1 & 0 \end{bmatrix}$, $B_{u,c} = [\frac{1}{J_{mg}}\ 0\ 0]^{\mathrm{T}}$, $B_{\omega,c} = I$. Here, the state variables x are chosen as

$$x = \begin{bmatrix} w_m - w_m^* \\ w_w - w_w^* \\ (\theta_m/i_g i_0 - \theta_w) - (\theta_m^*/i_g i_0 - \theta_w^*) \end{bmatrix} \tag{2}$$

where w is the error between the mathematical model and the actual IMT system, c_m is the motor damping, c_f is the driveshaft damping, k_f is the driveshaft stiffness, T_m is the motor torque, $J_v = J_m + m_v r_w^2$, $J_{mg} = J_m + J_g/i_g^2 i_0^2$, i_0 is the final drive ratio, i_g is the gear ratio, C_a is the air resistance coefficient, J_v is the vehicle inertia, J_g is the gearbox inertia, J_m is the motor inertia, w_g is the rotation speed of gearbox output shaft, w_m is the motor rotation speed, w_w is the rotation speed of wheel, θ_w is the wheel angle, θ_m is the motor output angle, θ_g is the gearbox output shaft angle. T_m^*, w_m^*, w_w^* and θ_m^*, which have star added to the variables, are the desired values of the corresponding variables, separately. The desired value of the state variables can be obtained by the following relationship if the desired wheel speed w_w^* is given.

$$\begin{aligned} &w_m^* = i_g i_0 w_w^*, \\ &\theta_m^*/i_g i_0 - \theta_w^* = T_{load}^*/k_f, \\ &T_m^* = c_m i_g i_0 w_w^* + T_{load}^*/i_g i_0 \end{aligned} \tag{3}$$

where T_{load}^* is the desired external load torque. Actually, the signals sampled by sensors are periodical with fixed sampling period T_s. Therefore, the IMT continuous-time model in (1) is transformed to following discrete-time form for vehicle on-board controller design

$$x(k+1) = A_d x(k) + B_{u,d} u(k) + B_{\omega,d}\omega(k) \tag{4}$$

where $A_d = e^{A_c T_s}$, $B_{u,d} = \int_0^{T_s} e^{A_c(T_s-\theta)} d\theta B_{u,c}$, $B_{\omega,d} = \int_0^{T_s} e^{A_c(T_s-\theta)} d\theta B_{\omega,c}$.

D. IMT System Modeling Considering Attack-Delays

Assuming that the attack-induced time-varying delays are bounded, and maximum delay $\tau_{\max}$ can be composed of ψT_s and ΥT_s as follows:

$$\tau_{\max} = (\psi + \Upsilon) T_s \tag{5}$$

where $\psi \in Z_+$ and $\Upsilon \in R_{[0,1)}$. By referring to Fig. 2, the IMT discrete-time system in (4) can be rewritten as the following nonlinear system to consider the effect of attack-delays on actual control inputs.

$$\begin{aligned} x(k+1) = {} & A_d x(k) + B_{u,d} u(k) + B_{\omega,d}\omega(k) \\ & + \Delta_{0,k}(u(k-1) - u(k)) + \cdots \\ & + \Delta_{\psi,k}(u(k-\psi-1) - u(k-\psi)) \end{aligned} \tag{6}$$

where

$$\Delta_{i,k} = \begin{cases} \int_0^{\tau_{k-i} - iT_s} e^{A_c(T_s-\theta)} d\theta B_{u,c}, 0 \le \tau_{k-i} - iT_s \le T_s \\ \int_0^{T_s} e^{A_c(T_s-\theta)} d\theta B_{u,c}, T_s \le \tau_{k-i} - iT_s \end{cases} \tag{7}$$

with $i = 0, 1, \ldots, \psi$.

The nonlinear integral part in (7) can be linearized as a finite summation and an infinitely small quantity by Taylor linear

series expansion as follows [44]:

$$\begin{aligned}\Delta(\varepsilon) &= \int_0^{\varepsilon} e^{A_c(T_s-\theta)}d\theta \\ &= -\sum_{m=1}^{h}\frac{(-\varepsilon)^m}{m!}A_c^{m-1}e^{A_cT_s} + \Theta^h.\end{aligned} \tag{8}$$

The approximation of (8) is obtained if ignoring residual Θ^h. The two intervals $0 \le \tau_{k-i} - iT_s \le T_s$ and $T_s \le \tau_{k-i} - iT_s$ in (7) represent the two delay patterns ΥT_s and T_s in a sampling interval. Therefore, nonlinear $\Delta_{i,k}$ can be rewritten as a combination of a set of linear vertices and vectors as shown below:

$$\Delta_{i,k} = \begin{cases} \sum_{l=1}^{h+1}\beta_{i,l}(k)\widehat{R}\sigma_{\Upsilon,l}B_{u,c}, \forall i = 0,1,\ldots,\psi-1 \\ \sum_{l=1}^{h+1}\beta_{i,l}(k)\widehat{R}\sigma_{\psi,l}B_{u,c}, \forall i = \psi \end{cases} \tag{9}$$

where $\forall l = 1,2,\ldots,h+1$, $\sum_{l=1}^{h+1}\beta_{i,l}(k) = 1$, $\beta_{i,l}(k) > 0$,

$$\widehat{R} = \left[0, \frac{(-1)^2}{1!}A_c^0 e^{A_cT_s}, \ldots, \frac{(-1)^{h+1}}{(h)!}A_c^{h-1}e^{A_cT_s}\right],$$

$$\sigma_{\psi,l} = \begin{cases} \sigma_{\psi,1} = [0\ 0\ \cdots\ 0]^{\mathrm{T}}, \\ \sigma_{\psi,2} = [T_s\ 0\ \cdots\ 0]^{\mathrm{T}}, \\ \vdots \\ \sigma_{\psi,h+1} = [T_s\ {T_s}^2\ \cdots\ {T_s}^h]^{\mathrm{T}}, \end{cases}$$

$$\sigma_{\Upsilon,l} = \begin{cases} \sigma_{\Upsilon,1} = [0\ 0\ \cdots\ 0]^{\mathrm{T}}, \\ \sigma_{\Upsilon,2} = [(\Upsilon T_s)\ 0\ \cdots\ 0]^{\mathrm{T}}, \\ \vdots \\ \sigma_{\Upsilon,h+1} = [(\Upsilon T_s)\ (\Upsilon T_s)^2\ \cdots\ (\Upsilon T_s)^h]^{\mathrm{T}}. \end{cases}$$

Therefore, $\xi(k) = [x^{\mathrm{T}}(k), u^{\mathrm{T}}(k-1), \ldots, u^{\mathrm{T}}(k-\psi-1)]^{\mathrm{T}}$ is employed as a new state vector to convert the nonlinear system (6) into a standard state-space model as follows:

$$\xi(k+1) = A_p(\alpha)\xi(k) + B_p(\alpha)u(k) + E_p\omega(k) \tag{10}$$

where

$$A_p(\alpha) = \begin{bmatrix} A_d & \Delta_{0,k}-\Delta_{1,k} & \cdots & \Delta_{\psi-1,k}-\Delta_{\psi,k} & \Delta_{\psi,k} \\ 0 & 0 & \cdots & 0 & 0 \\ 0 & I & \cdots & 0 & 0 \\ \vdots & \vdots & \ddots & \vdots & \vdots \\ 0 & 0 & \cdots & I & 0 \end{bmatrix},$$

$$B_p(\alpha) = \begin{bmatrix} B_{u,d}-\Delta_{0,k} \\ I \\ 0 \\ \vdots \\ 0 \end{bmatrix}, E_p = \begin{bmatrix} B_{\omega,d} \\ 0 \\ 0 \\ \vdots \\ 0 \end{bmatrix}.$$

There are $\psi+1$ uncertain terms $\Delta_{0,k}, \Delta_{1,k}, \ldots, \Delta_{\psi,k}$ in the system (10). Each item $\Delta_{i,k}$ generates $h+1$ terms as $\forall l = 1,2,\ldots,h+1$ shown in (9). Therefore, polytopic inclusion method is employed to describe the attack-delays by a convex polytope with $(h+1)^{\psi+1}$ vertices and (10) can be further expressed in the following form [34], [44].

$$\xi(k+1) = \sum_{i=1}^{s}\alpha_i\tilde{A}_{p,i}\xi(k) + \sum_{i=1}^{s}\alpha_i\tilde{B}_{p,i}u(k) + E_p\omega(k) \tag{11}$$

where $\sum_{i=1}^{s}\alpha_i = 1$, $s = (h+1)^{\psi+1}$.

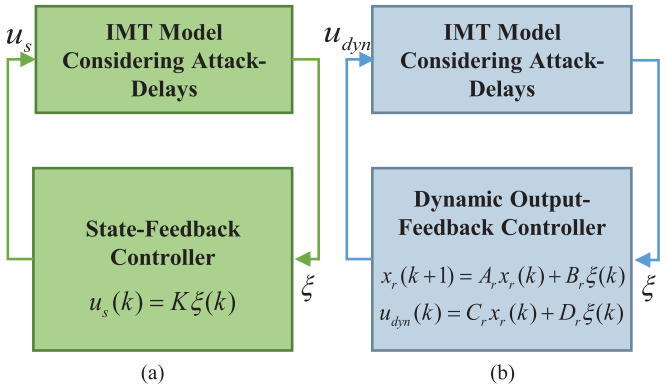

Fig. 3. Schematic diagram of closed-loop system. (a) State-feedback control, (b) Dynamic output-feedback control.

III. Dynamic Output-Feedback Closed-Loop System Design Considering Attack-Delays

A. Closed-Loop Control System Design

Figs. 3(a) and 3(b) show the schematic diagram of state-feedback closed-loop system and dynamic output-feedback closed-loop system. Compared with state-feedback control law $u_s(k) = K\xi(k)$, a dynamic vector $x_r(k)$ provides more freedom for a dynamic controller which can be expressed as follows:

$$\begin{cases} x_r(k+1) = A_r x_r(k) + B_r\xi(k), \\ u_{dyn}(k) = C_r x_r(k) + D_r\xi(k) \end{cases} \tag{12}$$

where A_r, B_r, C_r and D_r are the controller matrix. Furthermore, we can obtain the following dynamic output-feedback closed-loop system by employing a new state vector $X(k) = [\xi^{\mathrm{T}}(k), x_r^{\mathrm{T}}(k)]^{\mathrm{T}}$.

$$X(k+1) = A_{dyn}(\alpha)X(k) + E_{dyn}w(k) \tag{13}$$

where $A_{dyn}(\alpha) = \begin{bmatrix} A_p(\alpha)+B_p(\alpha)D_r & B_p(\alpha)C_r \\ B_r & A_r \end{bmatrix}$, $E_{dyn} = \begin{bmatrix} E_p \\ 0 \end{bmatrix}$.

The tracking error of wheel speed and the axle wrap rate are selected as controlled outputs to evaluate the speed synchronization performance and IMT powertrain system oscillations, which can be expressed as follows:

$$\begin{aligned} Z_{dyn1}(k) &= C_{dyn1}X(k), \\ Z_{dyn2}(k) &= C_{dyn2}X(k) \end{aligned} \tag{14}$$

where

$$C_{dyn1} = \left[C_{p1}\ 0\ 0\ 0\ \underbrace{[0\ \cdots\ 0]}_{\psi+1}\right],$$

$$C_{dyn2} = \left[C_{p2}\ 0\ 0\ 0\ \underbrace{[0\ \cdots\ 0]}_{\psi+1}\right],$$

with

$$C_{p1} = \begin{bmatrix} 0\ I\ 0\ \underbrace{[0\ \cdots\ 0]}_{\psi+1} \end{bmatrix},$$

$$C_{p2} = \begin{bmatrix} I/i_g i_0\ -I\ 0\ \underbrace{[0\ \cdots\ 0]}_{\psi+1} \end{bmatrix}.$$

B. Dynamic Output-Feedback Controller Design

The following performance is employed to ensure the stability of the IMT speed synchronization control system as well as the energy-to-peak performance of the closed-loop system, which is

$$\begin{aligned} \|Z_{dyn1}(k)\|_\infty &< \vartheta_1 \|w(k)\|_2, \\ \|Z_{dyn2}(k)\|_\infty &< \vartheta_2 \|w(k)\|_2 \end{aligned} \tag{15}$$

where $\|Z_{dyn1}(k)\|_\infty$ and $\|Z_{dyn2}(k)\|_\infty$ are the ∞-norm of $Z_{dyn1}(k)$ and $Z_{dyn2}(k)$, and $\|w(k)\|_2$ denotes the 2-norm of $w(k)$. ϑ_1 and ϑ_2 are the energy-to-peak performance indexes, which are used to constrain the impact of the external input $w(k)$ on the controlled output $Z_{dyn1}(k)$ and $Z_{dyn2}(k)$.

In order to obtain dynamic controller matrices A_r, B_r, C_r and D_r in (12), Theorem 1 is designed. Based on Theorem 1, the matrix inequality conditions for the closed-loop system in (13) satisfying Lyapunov stability and energy-to-peak performance are derived.

Theorem 1: Suppose that the controller in (12) is designed. The closed-loop system in (13) is asymptotically stable with two positive energy-to-peak performance indexes ϑ_1 and ϑ_2, if the matrices $S = \begin{bmatrix} S_{11} & S_{12} \\ * & S_{22} \end{bmatrix}$ and $M = \begin{bmatrix} M_{11} & \lambda_1 M_{11} \\ \lambda_2 M_{22} & M_{22} \end{bmatrix}$ satisfying following LMIs are solved.

$$\begin{bmatrix} -S_{11} & -S_{12} & S_{11}C_{p1}^{\mathrm{T}} \\ * & -S_{22} & S_{12}^{\mathrm{T}}C_{p1}^{\mathrm{T}} \\ * & * & -{\vartheta_1}^2 I \end{bmatrix} < 0, \tag{16}$$

$$\begin{bmatrix} -S_{11} & -S_{12} & S_{11}C_{p2}^{\mathrm{T}} \\ * & -S_{22} & S_{12}^{\mathrm{T}}C_{p2}^{\mathrm{T}} \\ * & * & -{\vartheta_2}^2 I \end{bmatrix} < 0, \tag{17}$$

$$\begin{bmatrix} S_{11} & S_{12} \\ * & S_{22} \end{bmatrix} > 0, \tag{18}$$

$$\begin{bmatrix} -S_{11} & -S_{12} & \Xi_1 & \Xi_2 & E_p \\ * & -S_{22} & \bar{B} + \lambda_2 \bar{A} & \lambda_1 \bar{B} + \bar{A} & 0 \\ * & * & \varpi_{11} & \varpi_{12} & 0 \\ * & * & * & \varpi_{22} & 0 \\ * & * & * & * & -I \end{bmatrix} < 0 \tag{19}$$

where $\forall i = 1, 2, \cdots (\lambda+1)^{\psi+1}$, $\Xi_1 = \tilde{A}_{p,i} M_{11} + \tilde{B}_{p,i}\bar{D} + \lambda_2 \tilde{B}_{p,i}\bar{C}$, $\Xi_2 = \lambda_1 \tilde{A}_{p,i} M_{11} + \lambda_1 \tilde{B}_{p,i}\bar{D} + \tilde{B}_{p,i}\bar{C}$, $\varpi_{11} = S_{11} - M_{11} - M_{11}^{\mathrm{T}}$, $\varpi_{12} = S_{12} - \lambda_1 M_{11} - \lambda_2 M_{22}^{\mathrm{T}}$, $\varpi_{22} = S_{22} - M_{22} - M_{22}^{\mathrm{T}}$, with $\bar{A} = A_r M_{22}$, $\bar{B} = B_r M_{11}$, $\bar{C} = C_r M_{22}$, $\bar{D} = D_r M_{11}$.

Proof: A Lyapunov function is selected as

$$L(k) = X^{\mathrm{T}}(k)\Omega X(k) \tag{20}$$

where the Lyapunov matrix Ω satisfies $\Omega = \Omega^{\mathrm{T}} > 0$, and the difference of the Lyapunov function can be expressed as follow:

$$\Delta L(k) = X^{\mathrm{T}}(k+1)\Omega X(k+1) - X^{\mathrm{T}}(k)\Omega X(k). \tag{21}$$

The energy-to-peak performance is achieved if the following condition holds [45]

$$L(k) - \sum_{i=0}^{k-1} w^{\mathrm{T}}(k) w(k) < 0. \tag{22}$$

Therefore, (22) is negative if we have

$$\begin{bmatrix} A_{dyn}^{\mathrm{T}}(\alpha)\Omega A_{dyn}(\alpha) - \Omega & A_{dyn}^{\mathrm{T}}(\alpha)\Omega E_{dyn} \\ * & E_{dyn}^{\mathrm{T}}\Omega E_{dyn} - I \end{bmatrix} < 0. \tag{23}$$

The condition (15) and (23) are described as follows by employing Schur complement.

$$\begin{bmatrix} -\Omega & \Omega A_{dyn}(\alpha) & \Omega E_{dyn} \\ * & -\Omega & 0 \\ * & * & -I \end{bmatrix} < 0, \tag{24}$$

$$\begin{bmatrix} -\Omega & C_{dyn1}^{\mathrm{T}} \\ * & -\vartheta_1^2 I \end{bmatrix} < 0, \tag{25}$$

$$\begin{bmatrix} -\Omega & C_{dyn2}^{\mathrm{T}} \\ * & -\vartheta_2^2 I \end{bmatrix} < 0. \tag{26}$$

Performing the congruence transformation to (24)−(26) with $\mathrm{diag}\{\Omega^{-1}, \Omega^{-1}, I\}$, $\mathrm{diag}\{\Omega^{-1}, I\}$, $\mathrm{diag}\{\Omega^{-1}, I\}$, and referring to [46], the following matrix inequalities can be obtained with $\Omega^{-1}{=}S$.

$$\begin{bmatrix} -S & A_{dyn}(\alpha)M & E_{dyn} \\ * & S - M - M^{\mathrm{T}} & 0 \\ * & * & -I \end{bmatrix} < 0, \tag{27}$$

$$\begin{bmatrix} -S & SC_{dyn1}^{\mathrm{T}} \\ * & -\vartheta_1^2 I \end{bmatrix} < 0, \tag{28}$$

$$\begin{bmatrix} -S & SC_{dyn2}^{\mathrm{T}} \\ * & -\vartheta_2^2 I \end{bmatrix} < 0 \tag{29}$$

where S is symmetric positive-definite matrix and

$$\begin{aligned} A_{dyn}(\alpha)M &= \begin{bmatrix} \Lambda_1 & \Lambda_2 \\ \bar{B} + \lambda_2 \bar{A} & \lambda_1 \bar{B} + \bar{A} \end{bmatrix} \\ &= \begin{bmatrix} A_p(\alpha) + B_p(\alpha) D_r & B_p(\alpha) C_r \\ B_r & A_r \end{bmatrix} \begin{bmatrix} M_{11} & \lambda_1 M_{11} \\ \lambda_2 M_{22} & M_{22} \end{bmatrix} \end{aligned} \tag{30}$$

where $\Lambda_1 = A_p(\alpha)M_{11} + B_p(\alpha)\bar{D} + \lambda_2 B_p(\alpha)\bar{C}$, $\Lambda_2 = \lambda_1 A_p(\alpha)M_{11} + \lambda_1 B_p(\alpha)\bar{D} + B_p(\alpha)\bar{C}$.

Therefore, the condition in (27) can be rewritten as follows:

$$\begin{bmatrix} -S_{11} & -S_{12} & \Lambda_1 & \Lambda_2 & E_p \\ * & -S_{22} & \bar{B} + \lambda_2 \bar{A} & \lambda_1 \bar{B} + \bar{A} & 0 \\ * & * & \varpi_{11} & \varpi_{12} & 0 \\ * & * & * & \varpi_{22} & 0 \\ * & * & * & * & -I \end{bmatrix} < 0. \tag{31}$$

In the reference of [34], [44], the delay-free nonlinear state-space in (10) can be expressed as (11) by polytopic inclusion method, thus (31) can be described by (19). Therefore, we can complete the proof. ■

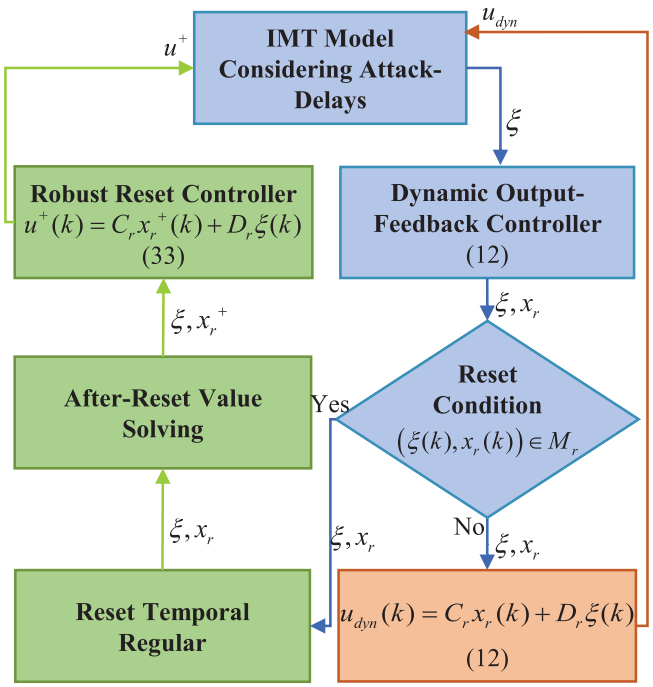

Fig. 4. Online algorithm flow of the robust reset control.

Finally, given a positive scalar ϑ_1, the minimum energy-to-peak performance ϑ_2 and the matrices $\bar{A}$, $\bar{B}$, $\bar{C}$, $\bar{D}$ can be obtained by solving following optimal problem:

$$\begin{aligned} &\min \vartheta_2^2 I, \\ &\text{s.t. } (16)-(19). \end{aligned} \tag{32}$$

Furthermore, the controller matrices can be calculated by $A_r=\bar{A}M_{22}^{-1}$, $B_r=\bar{B}M_{11}^{-1}$, $C_r=\bar{C}M_{22}^{-1}$, $D_r=\bar{D}M_{11}^{-1}$.

Remark 1: It should be stressed that the design of matrix $M=\begin{bmatrix} M_{11} & \lambda_1 M_{11} \\ \lambda_2 M_{22} & M_{22} \end{bmatrix}$ in Theorem 1 is different from the matrix $M=\begin{bmatrix} M_{11} & M_{12} \\ M_{12}^T & M_{22} \end{bmatrix}$ in [35] and [36], although they play the same role in matrix inequalities solving. In this paper, the form of M can reduce the complexity of matrix inequalities and obtain more suitable dynamic feedback matrices for the reset system by adjusting λ_1 and λ_2. In addition, the M in [35] and [36] is a special form of this paper.

IV. Robust Reset Controller Design

Fig. 4 shows the online algorithm flow of the reset robust controller. The overall control procedure is divided into online stage and offline stage.

As shown in Fig. 4, in the offline stage, the dynamic output-feedback controller matrices A_r, B_r, C_r, D_r satisfying energy-to-peak performance are calculated based on Theorem 1, which ensures the attack-delays robustness and speed tracking performance. Then they are fixed in the online stage. The reset control is activated when reset condition M_r is met, and this reset moment is designed as reset time k^+. Then, temporal regulation method is used to avoid large amounts of computing resources being occupied for a long time [42]. The duration of each reset and the interval time between each reset action are adjusted according to controller performance. Theorem 2 is used to calculate the after-reset value $x_r^+(k)$ and the dynamic controller states $x_r(k)$ are reset to $x_r^+(k)$. Moreover, the reset law is designed as follows:

$$\begin{cases} x_r(k+1)=A_r x_r(k)+B_r\xi(k), \\ x_r^+(k)=\rho\left(\xi(k), x_r(k)\right), \\ u^+(k)=C_r x_r^+(k)+D_r\xi(k) \end{cases} \tag{33}$$

where $x_r^+(k)$ is the after reset vector, M_r is the reset condition. And $\rho(\xi(k), x_r(k))$ is a function that determining the after-reset value. Therefore, the robust reset closed-loop system can be expressed as follows according to (13) and (33):

$$\begin{cases} X(k+1)=A_{dyn}(\alpha)X(k)+E_{dyn}w(k), \\ x_r^+(k)=\rho\left(X(k)\right). \end{cases} \tag{34}$$

The after-reset value $x_r^+(k)=\rho(\xi(k), x_r(k))$ can be obtained in terms of the condition in Theorem 2.

Theorem 2: For the stable system (34), if there exist matrices $H=\begin{bmatrix} H_{11} & \mu_1 H_{11} \\ \mu_2 H_{22} & H_{22} \end{bmatrix}$, F_p, F_r, F and positive-definite matrix $Q=\begin{bmatrix} Q_{11} & Q_{12} \\ * & Q_{22} \end{bmatrix}$, the after-reset value can be obtained by solving following optimal problem:

$$\begin{bmatrix} -Q_{11} & -Q_{12} & 0 & 0 \\ * & -Q_{22} & 0 & 0 \\ * & * & -I & 0 \\ * & * & * & -I \\ * & * & * & * \\ * & * & * & * \\ * & * & * & * \end{bmatrix}$$
$$\tilde{A}_{p,i}H_{11}+\tilde{B}_{p,i}D_r H_{11}+\mu_2\tilde{B}_{p,i}C_r H_{22}$$
$$B_r H_{11}+\mu_2 A_r H_{22}$$
$$\Phi_{11}^{\frac{1}{2}}H_{11}$$
$$\mu_2\Phi_{22}^{\frac{1}{2}}H_{22}$$
$$Q_{11}-H_{11}-H_{11}^{\mathrm{T}} \tag{35}$$

$$\begin{bmatrix} \mu_1\tilde{A}_{p,i}H_{11}+\mu_1\tilde{B}_{p,i}D_r H_{11}+\tilde{B}_{p,i}C_r H_{22} & E_p \\ \mu_1 B_r H_{11}+A_r H_{22} & 0 \\ \mu_1\Phi_{11}^{\frac{1}{2}}H_{11} & 0 \\ \Phi_{22}^{\frac{1}{2}}H_{22} & 0 \\ Q_{12}-\mu_1 H_{11}-\mu_2 H_{22}^{\mathrm{T}} & 0 \\ Q_{22}-H_{22}-H_{22}^{\mathrm{T}} & 0 \\ * & -I \end{bmatrix} < 0,$$

$$\begin{bmatrix} \gamma & * & * \\ \xi(k) & Q_{11} & * \\ F_p\xi(k)+F_r x_r(k)+F & Q_{12}^{\mathrm{T}} & Q_{22} \end{bmatrix} > 0, \tag{36}$$

$$\begin{bmatrix} Q_{11} & Q_{12} \\ * & Q_{22} \end{bmatrix} > 0, \tag{37}$$

$\forall i=1,2,\cdots(\lambda+1)^{\psi+1}$.

Proof: Consider a quadratic Lyapunov function for system to complete the proof below

$$V(k) = X^{\mathrm{T}}(k)PX(k) \tag{38}$$

where $P^{\mathrm{T}} = P > 0$. A cost function for evaluating system stability and robust performance is defined as follows:

$$\Psi(k) = X^{\mathrm{T}}(k)PX(k) - \sum_{i=0}^{k-1} w^{\mathrm{T}}(k)w(k). \tag{39}$$

A quadratic cost function for tracking error is defined as:

$$J(k^+) = \sum_{i=k^+}^{\infty} X^{\mathrm{T}}(k^+)\Phi X(k^+) \tag{40}$$

where $\Phi = \mathrm{diag}\{\Phi_{11}, \Phi_{22}\}$ and k^+ is the reset point time. We assume the relationship between $J(k^+)$, $\Psi(k^+)$ and the upper bound γ of them as following [47]

$$J(k^+) < \Psi(k^+) < \gamma. \tag{41}$$

By substituting the closed-loop system (34) into (39)−(41), $J(k^+) < \Psi(k^+)$ is equivalent to follows

$$\begin{bmatrix} A_{dyn}^{\mathrm{T}}(\alpha)PA_{dyn}(\alpha) - P + \Phi & A_{dyn}^{\mathrm{T}}(\alpha)PE_{dyn} \\ * & E_{dyn}^{\mathrm{T}}PE_{dyn} - I \end{bmatrix} < 0. \tag{42}$$

Applying Schur complement to (42), we can obtain the following matrix inequality.

$$\begin{bmatrix} -P^{-1} & 0 & A_{dyn}(\alpha) & E_{dyn} \\ * & -I & \Phi^{\frac{1}{2}} & 0 \\ * & * & -P & 0 \\ * & * & * & -I \end{bmatrix} < 0. \tag{43}$$

Pre-multiplying and post-multiplying (43) by $\mathrm{diag}\{I, I, P^{-1}, I\}$ and referring to [46], the following matrix inequality can be obtained.

$$\begin{bmatrix} -Q & 0 & A_{dyn}(\alpha)H & E_{dyn} \\ * & -I & \Phi^{\frac{1}{2}}H & 0 \\ * & * & Q - H - H^{\mathrm{T}} & 0 \\ * & * & * & -I \end{bmatrix} < 0 \tag{44}$$

where $Q = P^{-1}$. Therefore, the condition in (35) can be obtained considering the system in (11). Minimizing the upper bound γ leads to minimization of $J(k^+)$. Therefore, the condition in (41) can be converted to the following LMI solving problem by employing Schur complement [41].

$$\begin{bmatrix} Q & X(k^+) \\ * & \gamma \end{bmatrix} > 0. \tag{45}$$

Defining $x_r(k^+) = F_p\xi(k) + F_r x_r(k) + F$ and $\xi(k^+) = \xi(k)$, the conditions in (35)−(37) can be obtained. The Proof is thereby completed. ■

Therefore, after-reset value $x_r(k^+)$ can be solved by the following optimal problem:

$$\begin{aligned} &\min \gamma, \\ &s.t. (35) - (37). \end{aligned} \tag{46}$$

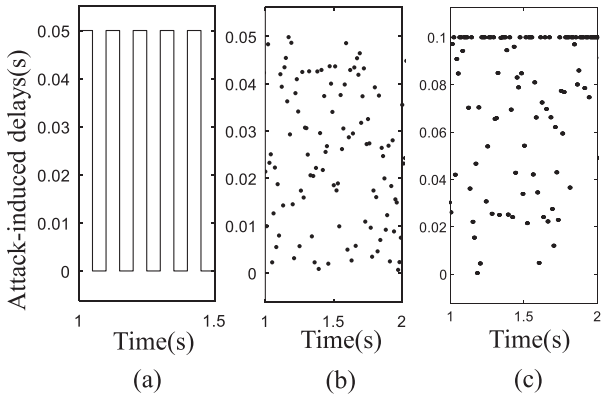

Fig. 5. Attack-induced delays. (a) Replay attack I, (b) Replay attack II, (c) Replay attack III.

TABLE I
MEANING AND VALUES OF MAIN PARAMETERS FOR IMT SYSTEM

Symbol	Meaning	Value
m_v	Vehicle mass	1094kg
i_0	Final drive ratio	3.667
i_g	Gear ratio	3.778
C_a	Air resistance coefficient	2.7N·m·s/rad
k_f	Driveshaft stiffness	6000N·m/rad
c_f	Driveshaft damping	42N·m·s/rad
c_m	Motor damping	0.15N·m·s/rad
J_w	Wheels inertia	5.38kg·m^2
J_g	Gearbox inertia	1.1828kg·m^2
J_m	Motor inertia	0.01kg·m^2
r_w	Wheel rolling radius	0.281m
g	Gravity acceleration	9.8m/s^2

V. SIMULATION RESULTS

In order to verify the effectiveness of the proposed robust reset controller, simulations using Matlab/Simulink (R2016a, MathWorks, Natick, MA, USA) environment are carried out. A process of upshifting and downshifting and a step upshift process are applied as driving conditions.

The designed simulation platform diagram is shown in Fig. 1. TCU is employed to calculate the tracking torque command. MCU and motor module receive this command through the in-vehicle CAN network. The real CAN message delays under replay attacks are imitated by random time-varying delays produced by the network module. The sampling time is set as 10 ms.

The impact of replay attacks on CAN message transmission is described by three attack-induced delays in Fig. 5. Fig. 5(a) represents a periodic attack in which each attack causes a delay of 50 ms. Figs. 5(b) and 5(c) describe two random attacks with maximum 50 ms and 100 ms attack-induced delays.

Table I lists the main parameters of an IMT powertrain system. Moreover, Table II shows the detailed controller parameters consisting of an MPC controller, the PD controller considering

TABLE II
CONTROLLER PARAMETERS WITH DIFFERENT DESIGN METHOD

Controller name	Design method	Gains or parameters name	Values
Model predictive controller	MPC toolbox	N_p, N_c	$N_p = 10$, $N_c = 4$
PD controller considering delays	Method in [48]	K_P,K_D	$K_P = -2$, $K_D = 0.065$
State-feedback robust controller	Method in [34]	K	[-0.380, -18.141, 296.482, -0.144, -0.094]
Dynamic output-feedback robust controller	Theorem 1	A_r	[0.002, 0.033, -0.461, 0.002, 0.000; 0.000, 0.000, -0.004, 0.000, 0.000; -0.000, -0.000, 0.001, -0.000, -0.000; -0.000, -0.010, 0.132, -0.001, -0.000; -0.000, -0.006, 0.087, -0.000, -0.000]
		B_r	[0.585, -0.187, -142.920, 0.057, 0.139; 0.001, 0.994, 0.610, 0.000, 0.000; 0.001, -0.009, 0.930, 0.000, 0.000; -0.381, -18.144, 296.437, -0.144, -0.094; -0.000, -0.002, -0.032, 1.000, -0.000]
		C_r	[-0.000, 0.002, -0.032, 0.000, 0.000]
		D_r	[-0.380, -18.141, 296.497, -0.144, -0.094]
Robust reset controller	Theorem 2	Φ_{11}	diag{0,1,0,0,0}
		Φ_{22}	10^{-9}diag{1,1,1,1,1}

time-varying delays referring to [48], the energy-to-peak delay-robust controller referring to [34] and the proposed controller. Among them, MPC prediction horizon $N_p = 10$ and control horizon $N_c = 4$. The minimum energy-to-peak performance index ϑ_2 of the proposed dynamic output-feedback controller is obtained as 0.423 by setting the performance index ϑ_1 to 0.1 with $\lambda_1 = 0.01$ and $\lambda_2 = 1$.

A. Comparisons With MPC in Effectiveness

MPC is getting more and more attention in dealing with constraints, time-varying systems, and tracking control. Especially in many chemical processes, it has been applied to deal with parameter uncertainty and time delay. The periodic attack I in Fig. 5(a) is employed to test the performance of the proposed controller with a model predictive controller. Figs. 6(a)−6(d) show the response of the motor torque, driveshaft torque, and the jitter of the powertrain during the speed synchronization control. It is necessary to mention that the MPC is designed for the powertrain system without any attack. However, in the simulation, the attack exists and the performance of designed MPC is affected significantly.

We can see from Fig. 6(a) that the model predictive controller and the proposed controller have similar control effects on the speed tracking. Fig. 6(b) shows the motor control signal calculated by MPC fluctuates greatly under replay attack I. In practice, these torque fluctuations should be avoided because they increase the load on the motor. However, the proposed controller has a more stable torque output, which preserves the oscillation damping capability under severe network congestion.

The axle wrap rate, which is the difference between the motor speed divided by the gear ratios and wheel speed, is used to characterize the jitter of the powertrain in engineering. Passenger ride comfort and drive shaft life are affected by this jitter. Therefore, the controller robustness can be indicated by the fluctuation frequency and peak value of the axle wrap rate. The warp rate responses of two controllers are shown in Fig. 6(c). We can see that the powertrain system under MPC shakes violently during shift. However, the proposed controller fluctuates slightly at the beginning and end of the upshifting and downshifting, robustness is improved compared with the MPC. As shown in Fig. 6(d), the driveshaft torque of MPC violently oscillates. However, the driveshaft torque response under the proposed controller has little oscillation compared with MPC. From the application prospective, passengers are sensitive to the driveshaft torque vibration. The proposed controller shows its good damping performance.

B. Comparisons With PD Controller Considering Time-Varying Delays in Effectiveness

PID controllers are widely used in industrial control as a classical feedback loop component due to its flexibility. We next verify the effectiveness of the proposed robust reset controller compared to the PD controller considering network delays referring to [48]. Figs. 7(a)−7(d) show the comparisons of proposed controller and PD controller under the process of upshifting and downshifting with maximum attack-delays of 50 ms in the control communication loop as shown in Fig. 5(b).

Fig. 7(a) shows that the proposed controller has a shorter rise time than the PD controller in speed tracking, which shows the proposed method have better speed synchronization capability in upshifting and downshifting conditions. Fig. 7(b) shows the motor torque response. The motor control signal calculated by PD controller in [48] fluctuates greatly, but the output signal calculated by the proposed controller is relatively stable. It needs to be further explained that during the upgrade phase of 0-2 s,

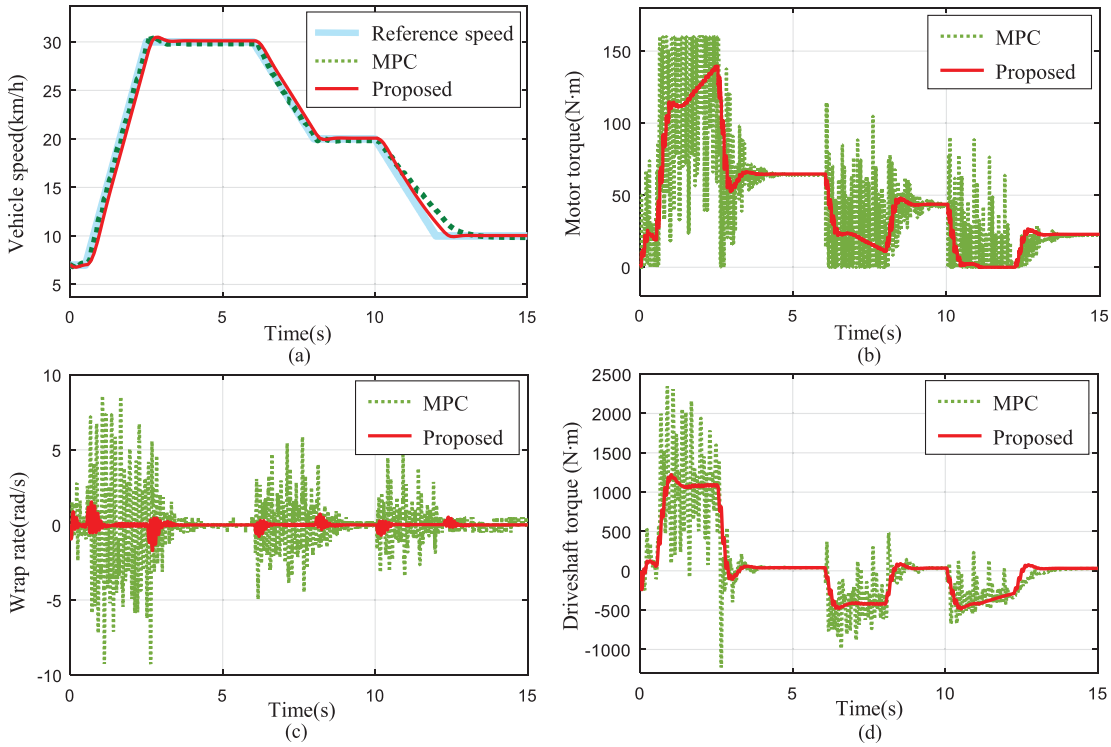

Fig. 6. The control performance under replay attack I.

9

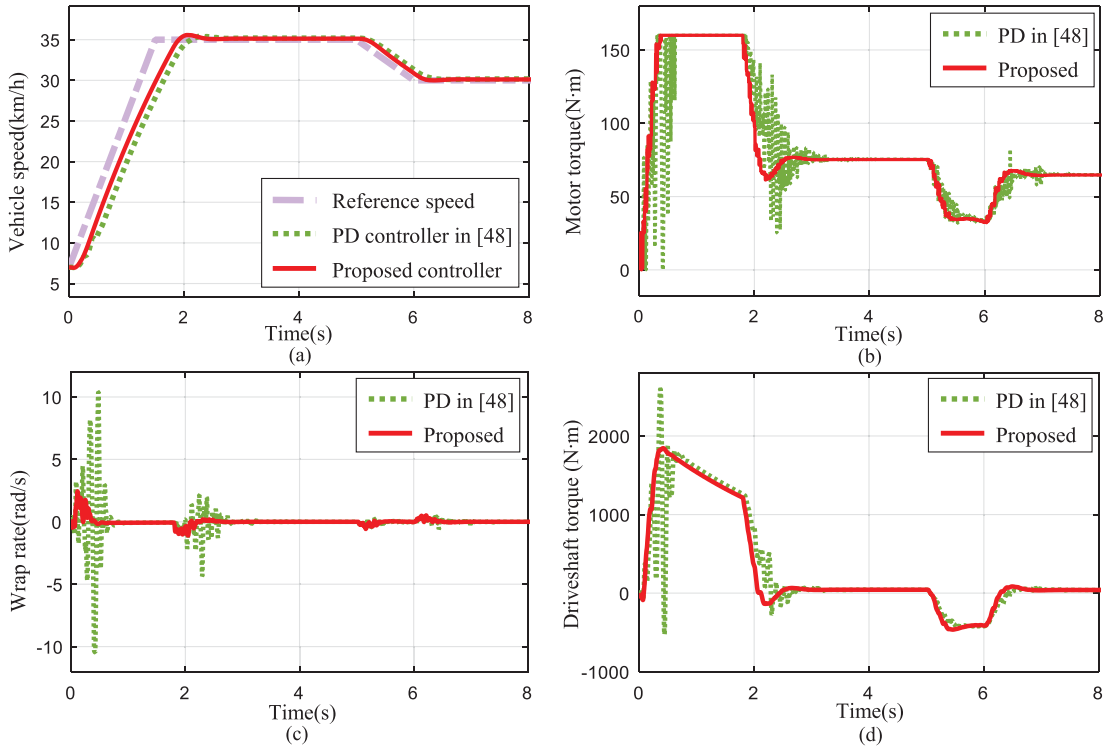

Fig. 7. The control performance under replay attack II.

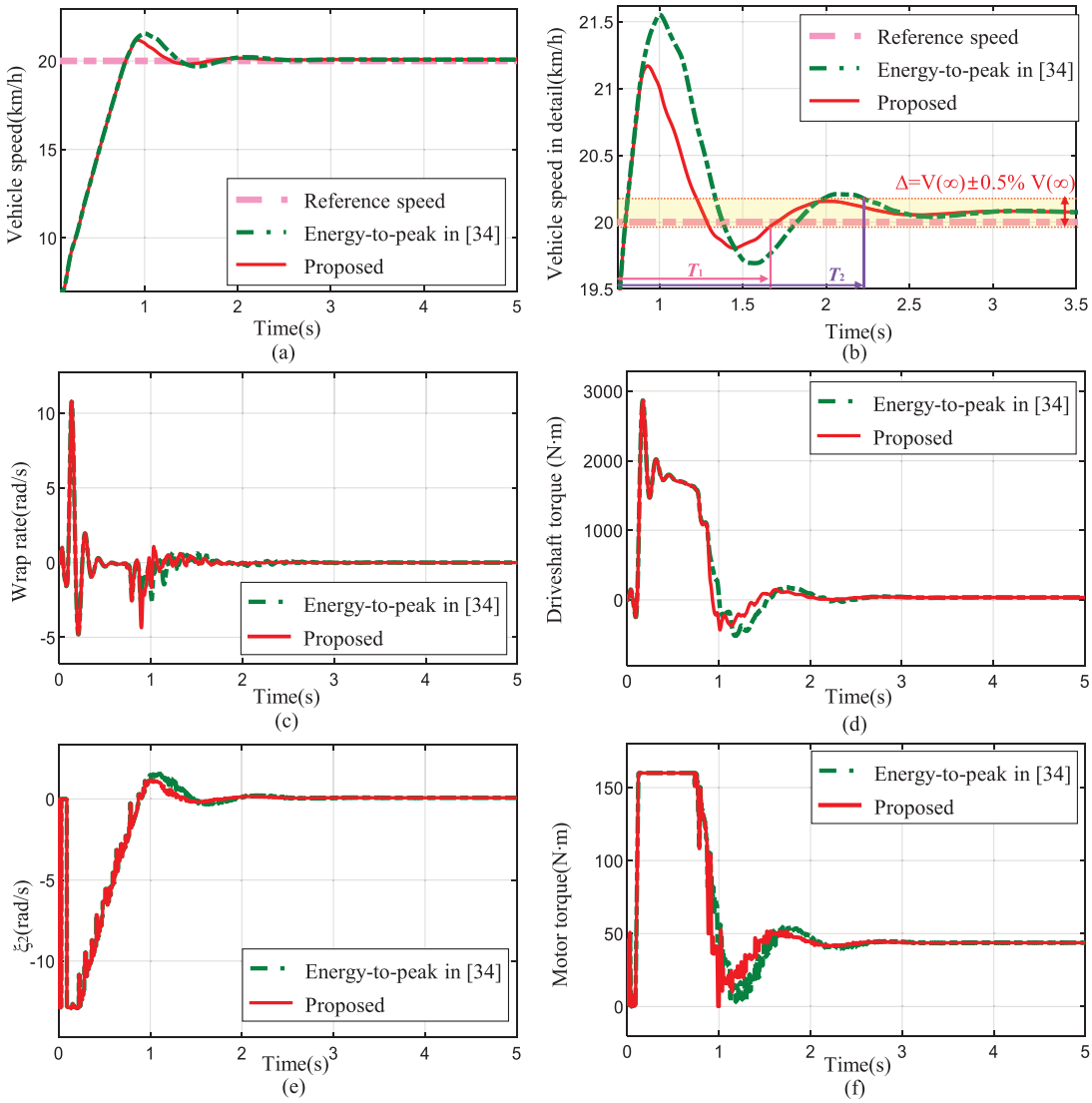

Fig. 8. The performance of the robust reset control under replay attack III.

the motor has a stable interval without jitter due to actuator saturation.

The warp rate responses of the two controllers are shown in Fig. 7(c). We can see that the PD controller causes a large oscillation in powertrain system at the beginning and end of the shift. The same result can be obtained from Fig. 7(d). The controller we proposed shows its good damping performance and the driveshaft torque has little oscillation. Therefore, the robustness is obviously improved compared with the PD controller considering delays.

C. Comparisons With Energy-to-Peak Delay-Robust Controller in High-Efficiency

In order to verify the improvement, we test the proposed robust reset controller in step upshift under replay attack III in Fig. 5(c), in contrast with the energy-to-peak controller in [34]. Comparison results are shown in Figs. 8 and 9. Figs. 8(a) and 8(b) show the speed synchronization performance and its details. Furthermore, the proposed controller reaches its peak 21.17 km/h at 0.93 s and the settling time is T_1=1.67 s. The energy-to-peak controller reaches the peak 21.55 km/h at 1.01 s. It first enters and then stays within the error band at T_2=2.23 s. Table III depicts the overshoot and setting time of the two controller. In addition, the relative improvement is detailed. Table III shows the proposed controller has significant performance improvements in speed tracking compared to [34] when replay attack III happens.

TABLE III
RESPONSE PERFORMANCE INDICATORS AND RELATIVE IMPROVEMENT

Response characteristic	Overshoot	Settling time
Energy-to-peak controller	1.47km/h	2.23s
Robust reset controller	1.09km/h	1.67s
Relative improvement	25.9%	25.1%

Fig. 8(c) shows that the responses of the two controller oscillate similarly and are asymptotically stable. Proposed controller shows a peak at the beginning of the reset controller. The oscillation indicates that there are vibrations on the

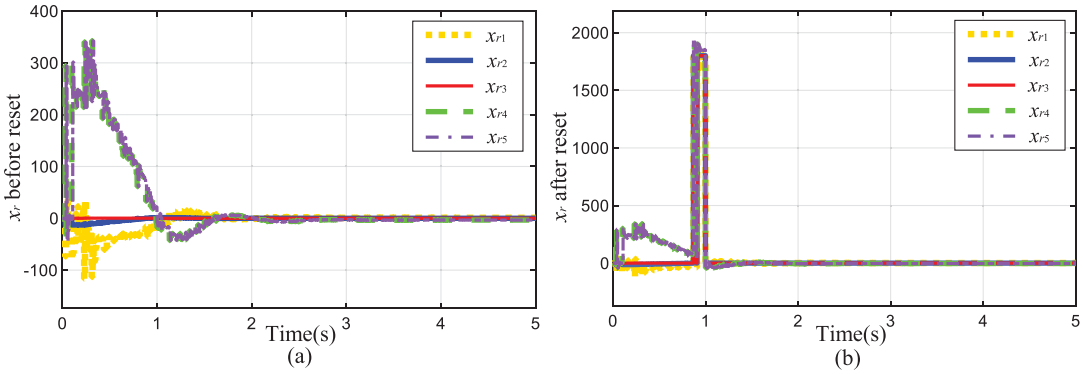

Fig. 9. The response of the dynamic vectors x_r under replay attack III.

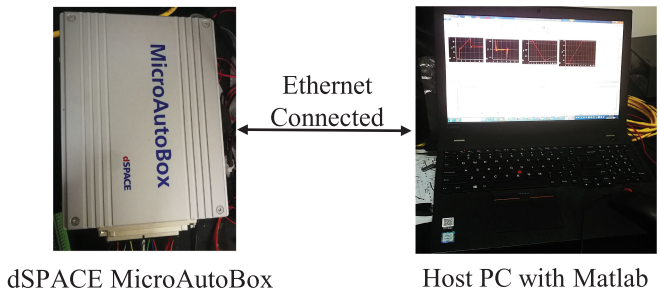

Fig. 10. HIL test system.

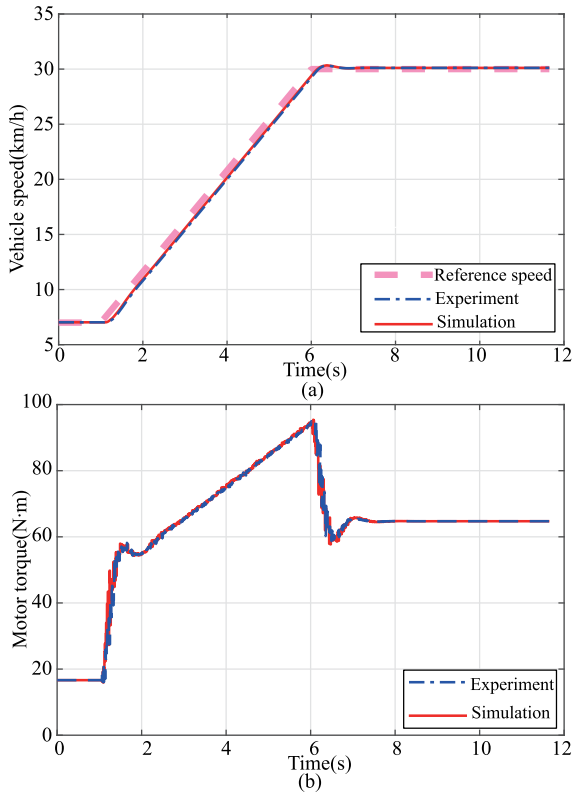

Fig. 11. Comparison of experiment and simulation results.

powertrain. Figs. 8(a)−8(c) shows that the proposed controller has better tracking performance than energy-to-peak controller with similar powertrain vibration. Due to excessive delays caused by a replay attack, the driveshaft torque and the motor torque response of the two controllers oscillate before reaching steady state as shown in Figs. 8(d) and 8(f). We can see that the proposed controller has a faster steady-state response. Compared to the energy-to-peak controller in [34], the proposed controller achieves better tracking performance with a smaller overshoot and a faster response when attack happened.

The difference between w_w and w_w^* is expressed in terms of $\xi_2(k)$. Furthermore, $w_w > w_w^*$ represents that the actual speed is bigger than the ideal speed, which means the appearance of overshoot in speed tracking. $\xi_2(k) > 0.07(rad/s)$ is selected as the condition for the reset control to be triggered. Furthermore, the response of $\xi_2(k)$ is shown in Fig. 8(e).

Figs. 9(a) and 9(b) show the before-reset states and after-reset vectors x_r which is calculated online by Theorem 2. The before-reset vectors in Fig. 9(a) will be replaced by x_r^+ when the reset condition is satisfied. Then the after-reset vectors in Fig. 9(b) is obtained.

VI. Experiment Under HIL Condition

The controller should guarantee its real-time control performance under a replay attack for further applied to real connected cars. Therefore, we set up a HIL online experiment based on a dSPACE MicoAutoBox simulator to verify its real-time and control effects under severe CAN information congestion.

In the HIL experiments, as shown in Fig. 10, a dSPACE MicoAutoBox and a host personal computer (PC) are employed. A TCU node, an MCU & motor node, an IMT powertrain node, a controller network module, a random delays generation module, a dynamic output-feedback controller combined a robust reset controller are loaded into the dSPACE MicoAutoBox, which is a real-time digital test system. The host PC is used to show the real-time test results.

Experimental conditions are set to step speed tracking from 7 km/h to 30 km/h under replay attack II in Fig. 5. Figs. 11(a) and 11(b) show the comparison of experimental and simulation results of speed tracking and motor torque. Fig. 11 shows that the simulation results are agree with the experimental results. The experimental results and simulation on IMT speed synchronization control prove the correctness and effectiveness of the proposed dynamic output-feedback combined with robust reset controller.

VII. Conclusion

In this work, we improved the IMT speed synchronization control system of a connected car under a replay attack. The controller design procedure was divided into offline part and online part. Firstly, the random time-varying delays generated by a replay attack on in-vehicle CAN were modeled by polytopic inclusion using Taylor series expansion. Secondly, a closed-loop model of the speed synchronization system considering a reset action was established. Thirdly, the control matrices of the dynamic output-feedback controller based on energy-to-peak performance were calculated offline by solving a set of LMIs, which were used for the online step tracking. Fourthly, the after-reset value was obtained by solving a set of LMI optimization problems online, which was used to replace the states of the dynamic controller. The simulation and experimental results are summarized as follows: 1) The proposed controller was more effective than MPC and PD control considering delays in speed tracking performance and oscillation damping performance. 2) The cost function considering known input w was proposed for the establishment of the reset controller and the proposed controller was more efficient than [34] with smaller overshoot and shorter settling time. 3) The HIL real-time experiment demonstrated that simulation results match the experimental results well. Based on this research, we will carry out more research in the aspects of multi-actuator reset control and collaboration with attack detection in [49], [50] in the future.

References

[1] A. Osseiran *et al.*, "Scenarios for 5 G mobile and wireless communications: The vision of the METIS project," *IEEE Commun. Mag.*, vol. 52, no. 5, pp. 26–35, May 2014.

[2] C. Wang *et al.*, "Cellular architecture and key technologies for 5 G wireless communication networks," *IEEE Commun. Mag.*, vol. 52, no. 2, pp. 122–130, Feb. 2014.

[3] M. Gerla, E. Lee, G. Pau, and U. Lee, "Internet of vehicles: From intelligent grid to autonomous cars and vehicular clouds," in *Proc. IEEE World Forum Internet Things*., 2014, pp. 241–246.

[4] K. H. Johansson, M. Törngren, and L. Nielsen, "Vehicle applications of controller area network," in *Handbook of Networked and Embedded Control Systems*. Berlin, Germany: Springer, 2005, pp. 741–765.

[5] P. Kleberger, T. Olovsson, and E. Jonsson, "Security aspects of the in-vehicle network in the connected car," in *Proc. IEEE Intell. Veh. Symp.*, 2011, pp. 528–533.

[6] R. Coppola and M. Morisio, "Connected car: Technologies, issues, future trends," *ACM Comput. Surv.*, vol. 49, no. 3, pp. 1–36, 2016.

[7] T. Hoppe and J. Dittman, "Sniffing/replay attacks on CAN buses: A simulated attack on the electric window lift classified using an adapted CERT taxonomy," in *Proc. 2nd Workshop Embedded Syst. Secur.*, 2007, pp. 1–6.

[8] C. Stephen, M. Damon, and A. Danny, "Comprehensive experimental analyses of automotive attack surfaces," in *Proc. USENIX Secur. Symp.*2011, pp. 77–92.

[9] M. Pal-Stefan and G. Bogdan, "Security shortcomings and countermeasures for the SAE J1939 commercial vehicle bus protocol," *IEEE Trans. Veh. Technol.*, vol. 67, no. 5, pp. 4325–4339, May 2018.

[10] K. Tae Un, S. H. Min, J. Seonghoon, and K. H. Kang, "Automated reverse engineering and attack for CAN using OBD-II," in *Proc. IEEE Veh. Technol. Conf.*, 2018, pp. 1–7.

[11] K. Karl, C. Alexei, and R. Franziska, "Experimental security analysis of a modern automobile," in *Proc. IEEE Symp. Secur. Privacy*, 2010, pp. 447–462.

[12] S. Woo, H. J. Jo, and D. H. Lee, "A practical wireless attack on the connected car and security protocol for in-vehicle CAN," *IEEE Trans. Intell. Transp. Syst.*, vol. 16, no. 2, pp. 993–1006, Apr. 2015.

[13] K. Koscher *et al.*, "Experimental security analysis of a modern automobile," in *Proc. IEEE Symp. Secur. Privacy*, 2010, pp. 447–462.

[14] B. Groza and S. Murvay, "Efficient protocols for secure broadcast in controller area networks," *IEEE Trans. Ind. Informat.*, vol. 9, no. 4, pp. 2034–2042, Nov. 2013.

[15] C. Lin and A. Sangiovanni-Vincentelli, "Cyber-security for the controller area network (CAN) communication protocol," in *Proc. IEEE Int. Conf. Cyber Secur.*, 2012, pp. 1–7.

[16] L. Zhang, Y. Shi, T. Chen, and B. Huang, "A new method for stabilization of networked control systems with random delays," *IEEE Trans. Autom. Control*, vol. 50, no. 8, pp. 1177–1181, Aug. 2005.

[17] H. S. Park, Y. H. Kim, D.-S. Kim, and W. H. Kwon, "A scheduling method for network-based control systems," *IEEE Trans. Control Syst. Technol.*, vol. 10, no. 3, pp. 318–330, May 2002.

[18] M. M. B. Gaid, A. Cela, and Y. Hamam, "Optimal integrated control and scheduling of networked control systems with communication constraints: Application to a car suspension system," *IEEE Trans. Control Syst. Technol.*, vol. 14, no. 4, pp. 776–787, Jul. 2006.

[19] K. Liu, E. Fridman, and L. Hetel, "Network-based control via a novel analysis of hybrid systems with time-varying delays," in *Proc. IEEE 51st Conf. Decis. Control*, 2012, pp. 3886–3891.

[20] A. Barreiro and A. Baños, "Delay-dependent stability of reset systems," *Automatica*, vol. 46, no. 1, pp. 216–221, 2010.

[21] A. Banos and A. Barreiro, "Delay-independent stability of reset systems," *IEEE Trans. Autom. Control*, vol. 54, no. 2, pp. 341–346, Feb. 2009.

[22] M. A. Davó, F. Gouaisbaut, A. Baños, S. Tarbouriech, and A. Seuret, "Stability of time-delay reset control systems with time-dependent resetting law," *IFAC-PapersOnLine*, vol. 48, no. 27, pp. 371–376, 2015.

[23] A. Baños and A. Barreiro, "Delay-independent stability of reset control systems," in *Proc. IEEE IECON 32nd Annu. Conf. Ind. Electron.*, 2006, pp. 665–670.

[24] A. Baños, F. Perez, and J. Cervera, "Network-based reset control systems with time-varying delays," *IEEE Trans. Ind. Inform.*, vol. 10, no. 1, pp. 514–522, Feb. 2014.

[25] D. Wu, D. C. Aliprantis, and K. Gkritza, "Electric energy and power consumption by light-duty plug-in electric vehicles," *IEEE Trans. Power Syst.*, vol. 26, no. 2, pp. 738–746, May 2011.

[26] Y. Hori, "Future vehicle driven by electricity and control-research on four-wheel-motored 'UOT electric march II'," *IEEE Trans. Ind. Electron.*, vol. 51, no. 5, pp. 954–962, Oct. 2004.

[27] Z. Shuai, H. Zhang, J. Wang, J. Li, and M. Ouyang, "Lateral motion control for four-wheel-independent-drive electric vehicles using optimal torque allocation and dynamic message priority scheduling," *Control Eng. Pract.*, vol. 24, pp. 55–66, 2014.

[28] W. Cao *et al.*, "Speed synchronization control for integrated automotive motor-transmission powertrains over CAN through a co-design methodology," *IEEE Access*, vol. 6, pp. 14 106–14 117, 2018.

[29] X. Xu, P. Dong, Y. Liu, and H. Zhang, "Progress in automotive transmission technology," *Automot. Innov.*, vol. 1, no. 3, pp. 187–210, 2018.

[30] X. Lu, W. Guo, S. Wang, and X. Xu, "Application of shift control parameter adaption strategy for automatic transmission," *Trans. Chin. Soc. Agricultural Eng.*, vol. 31, no. 12, pp. 83–91, 2015.

[31] C.-Y. Tseng and C.-H. Yu, "Advanced shifting control of synchronizer mechanisms for clutchless automatic manual transmission in an electric vehicle," *Mechanism Mach. Theory*, vol. 84, pp. 37–56, 2015.

[32] Y.-K. Kim, H.-W. Kim, I.-S. Lee, S. Park, and H. Mok, "A speed control for the reduction of the shift shocks in electric vehicles with a two-speed AMT," *J. Power Electron.*, vol. 16, no. 4, pp. 1355–1366, 2016.

[33] C. F. Caruntu, M. Lazar, R. H. Gielen, P. Van den Bosch, and S. Di Cairano, "Lyapunov based predictive control of vehicle drivetrains over CAN," *Control Eng. Pract.*, vol. 21, no. 12, pp. 1884–1898, 2013.

[34] X. Zhu, H. Zhang, D. Cao, and Z. Fang, "Robust control of integrated motor-transmission powertrain system over controller area network for automotive applications," *Mech. Syst. Signal Process.*, vol. 58, pp. 15–28, 2015.

[35] X. Li, X. Xu, H. Zhang, P. Dong, and Y. Liu, "DOS-robust dynamic speed tracking controller for an integrated motor-gearbox powertrain system of a connected car," in *Proc. 3rd Conf. Veh. Control Intell.*, 2019, pp. 1–6.

[36] X. Xu, X. Li, H. Zhang, and J. Zhou, "Event-triggered robust control of an integrated motor-gearbox powertrain system for a connected vehicle under CAN and DOS-induced delays," in *Proc. SAE Intell. Connected Veh. Symp.* SAE Int., Feb. 2020.

[37] Y. Liu, X. Zhu, H. Zhang, and M. Basin, "Improved robust speed tracking controller design for an integrated motor-transmission powertrain system over controller area network," *IEEE/ASME Trans. Mechatronics*, vol. 23, no. 3, pp. 1404–1414, Jun. 2018.

[38] W. Cao, H. Liu, C. Lin, Y. Chang, Z. Liu, and A. Szumanowski, "Speed synchronization control of integrated motor-transmission powertrain over can through active period-scheduling approach," *Energies*, vol. 10, no. 11, 2017, Art. no. 1831.
[39] A. Baños, J. Carrasco, and A. Barreiro, "Reset times-dependent stability of reset control systems," *IEEE Trans. Autom. Control*, vol. 56, no. 1, pp. 217–223, Jan. 2011.
[40] J. Clegg, "A nonlinear integrator for servomechanisms," *Trans. Amer. Inst. Elect. Eng., Part II: Appl. Ind.*, vol. 77, no. 1, pp. 41–42, 1958.
[41] N. Vafamand and A. Khayatian, "Model predictive-based reset gain-scheduling dynamic control law for polytopic LPV systems," *ISA Trans.*, vol. 81, pp. 132–140, 2018.
[42] V. Ghaffari, P. Karimaghaee, and A. Khayatian, "Reset law design based on robust model predictive strategy for uncertain systems," *J. Process Control*, vol. 24, no. 1, pp. 261–268, 2014.
[43] S. Woo, H. J. Jo, and D. H. Lee, "A practical wireless attack on the connected car and security protocol for in-vehicle CAN," *IEEE Trans. Intell. Transp. Ssystems*, vol. 16, no. 2, pp. 993–1006, Apr. 2015.
[44] Z. Shuai, H. Zhang, J. Wang, J. Li, and M. Ouyang, "Combined AFS and DYC control of four-wheel-independent-drive electric vehicles over CAN network with time-varying delays," *IEEE Trans. Veh. Technol.*, vol. 63, no. 2, pp. 591–602, Feb. 2014.
[45] H. Zhang, Y. Shi, and J. Wang, "Observer-based tracking controller design for networked predictive control systems with uncertain Markov delays," *Int. J. Control*, vol. 86, no. 10, pp. 1824–1836, 2013.
[46] H. Zhang, Y. Shi, and B. Mu, "Optimal H_∞-based linear-quadratic regulator tracking control for discrete-time takagi-sugeno fuzzy systems with preview actions," *J. Dyn. Syst., Meas., Control*, vol. 135, no. 4, 2013, Art. no. 0 44501.
[47] G. Zhao, D. Nešić, Y. Tan, and J. Wang, "Open problems in reset control," in *Proc. 52nd IEEE Conf. Decis. Control*, 2013, pp. 3326–3331.
[48] Á. Cuenca, J. Salt, A. Sala, and R. Pizá, "A delay-dependent dual-rate PID controller over an ethernet network," *IEEE Trans. Ind. Informat.*, vol. 7, no. 1, pp. 18–29, Feb. 2011.
[49] H. Zhang and J. Wang, "Active steering actuator fault detection for an automatically-steered electric ground vehicle," *IEEE Trans. Veh. Technol.*, vol. 66, no. 5, pp. 3685–3702, May 2017.
[50] Z. Ju, H. Zhang, and Y. Tan, "Deception attack detection and estimation for a local vehicle in vehicle platooning based on a modified UFIR estimator," *IEEE Internet Things J.*, vol. 7, no. 5, pp. 3693–3705, May 2020.

Xiangyang Xu received the B.Sc. degree and the M.Sc. degree in vehicle engineering, Beijing Institute of Technology, Beijing, China, in 1987 and 1990, respectively, and the Ph.D. degree in mechatronic engineering, Harbin Institute of Technology, Harbin, China, in 1999.

From 1998 to 1999, he was a Visiting Scholar at Daimler AG, Stuttgart, Germany. From 1990 to 2002, he is a staff of College of Automotive Engneering, Harbin Institute of Technology. He is a Professor of School of Transportation Science and Technology, Beihang University since 2002.

Prof. Xu is a member of the Advisory Board, Innovation Automotive Transmissions, Hybrid & Electrical Drives, International CTI Symposium and Exhibition (Berlin, Shanghai). He serves as a Fellow of SAE-China, an Executive member of SAE-China, a Deputy Secretary-General for SAE-China of Gear Technology Branch, a Deputy Secretary-General for China Gear Manufacturer Association (CGMA), the Director of Beijing Key Lab for High Efficiency and System Control of New Energy Resource Vehicle, an Executive Deputy Director of National Engineering Research Center for Passenger Car Automatic Transmission (NECPCAT). He was awarded a Best Paper Award by the 2019 SAE International Intelligent and Connected Vehicles Symposium. His research interests include transmission technology, hybrid and EV drive.

Xiang Li received the B.Sc. degree in vehicle engineering from the Nanjing University of Aeronautics and Astronautics, Nanjing, China, in 2016. She is currently working toward the Ph.D. degree in vehicle dynamics at the School of Transportation Science and Engineering, Beihang University, Beijing, China.

She is a recipient of 2019 SAE International Intelligent and Connected Vehicles Symposium Best Paper Award. Her research interests include networked control systems, cyber security of cyber-physical systems, autonomous vehicles, and vehicle dynamics and control.

Dong Peng received the B.S. degree in industrial engineering from Shandong University, Shandong, China, in 2008, the M.S. degree in vehicle engineering from Beihang University (BUAA), Beijing, China, in 2011, and the Ph.D. degree in mechanical engineering from Ruhr-University Bochum, Germany, in 2015.

He is currently an Associate Professor with the School of Transportation Science and Engineering, Beihang University. His research interests include powertrain system of green vehicles, design and control of vehicle transmission, and reliability of transmission system.

Yue Liu received the B.Sc. degree in automotive engineering from the Henan University of Science and Technology, Luo Yang, China, in 2016. She is currently working toward the Ph.D. degree in vehicle dynamics at the School of Transportation Science and Engineering, Beihang University, Beijing, China.

Her research interests include automation-driver interaction, vehicle dynamics and advanced control, and multivehicle cooperative control problems.

Hui Zhang (Senior Member, IEEE) received the B.Sc. degree in mechanical design manufacturing and automation from the Harbin Institute of Technology at Weihai, Weihai, China in 2006, the M.Sc. degree in automotive engineering from Jilin University, Changchun, China in 2008, and the Ph.D. degree in mechanical engineering from University of Victoria, Victoria, BC, Canada in 2012.

Dr. Zhang is a recipient of 2017 IEEE Transactions on Fuzzy Systems Outstanding Paper Award, 2018 SAE Ralph R. Teetor Educational Award, IEEE Vehicular Technology Society 2019 Best Vehicular Electronics Paper Award, and 2019 SAE International Intelligent and Connected Vehicles Symposium Best Paper Award. He is a member of SAE International, a senior member of IEEE and a member of ASME. Dr. Zhang serves as an Associate Editor for IEEE Transactions on Vehicular Technology, Journal of The Franklin Institute, SAE International Journal of Connected and Automated Vehicles, and ASME Transactions Journal of Dynamic Systems, Measurement and Control; Board member of International Journal of Hybrid and Electric Vehicles, Mechanical Systems and Signal Processing.